Saraogi et al., http://www.jcb.org/cgi/content/full/jcb.201311028/DC1

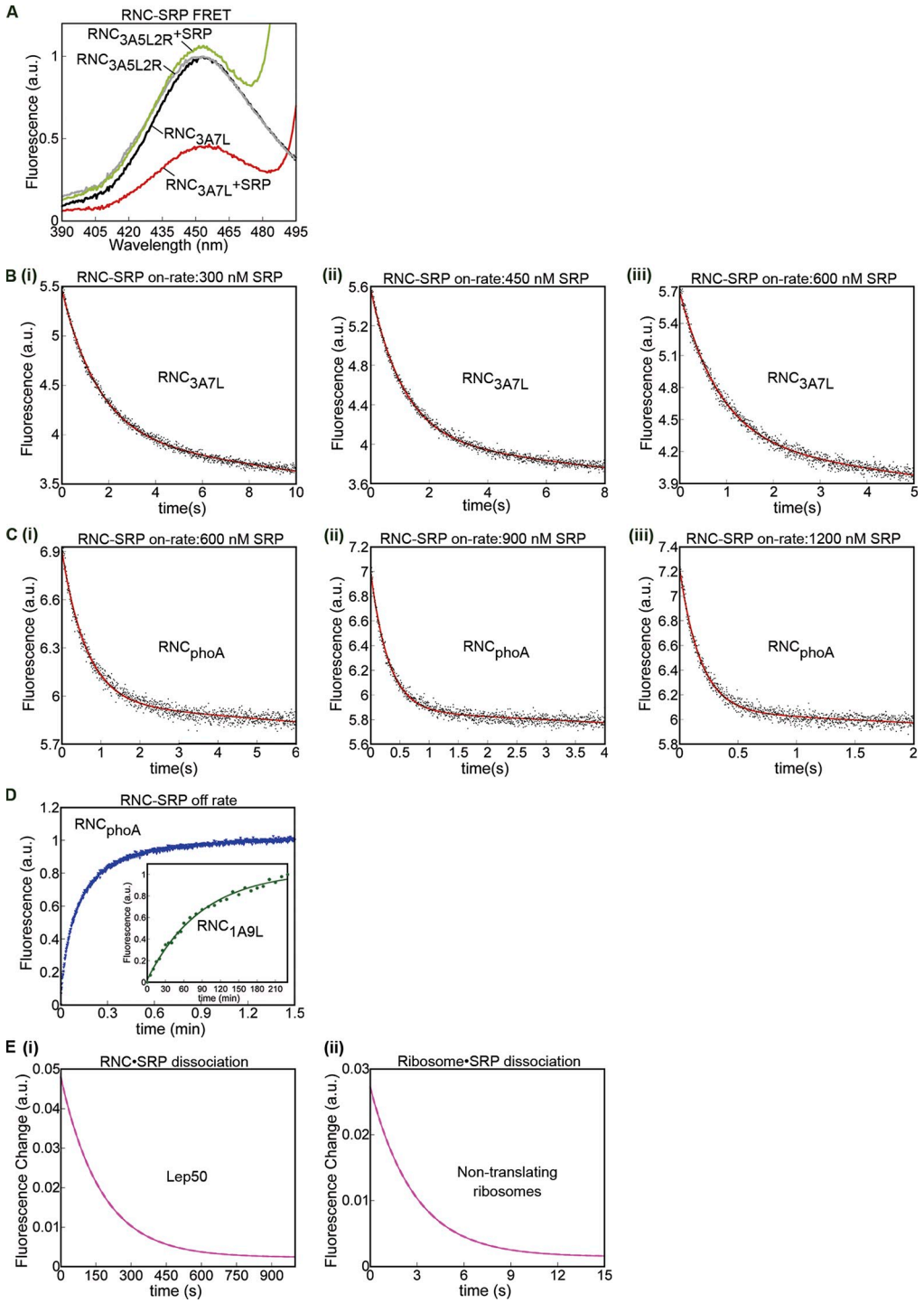

Figure S1. **Equilibrium and dynamics of RNCs binding to SRP.** (A) Change in donor fluorescence when 25 nM Cm-labeled wt-RNC (RNC_{3A7L}) or mt-RNC (RNC_{3A5L2R} containing two arginines into the signal sequence) was treated with 50 nM or 424 nM, respectively, of BODIPY-FL–labeled SRP 421. (B) Time courses for association of RNC_{3A7L} with 300, 450, and 600 nM SRP. (C) Time courses for association of RNC_{phoA} with 600, 900, and 1,200 nM SRP. For B and C, the observed rate constants obtained from Eq. 3 were used to generate Fig. 2 C. (D) A magnification of the plot for dissociation of RNC_{phoA} from SRP (Fig. 2 D) showing the biphasic behavior of RNC_{phoA}. The time course for phoA was fit to a double exponential (Eq. 5b) to give dissociation rate constants of 0.25 ± 0.023 s^{-1} and 0.053 ± 0.006 s^{-1}. The amplitudes for the two phases were 40% and 60%, respectively. Although the biphasic nature of SRP–RNC_{phoA} dissociation persisted as the targeting reaction progressed, the two phases responded similarly to FtsY. Therefore, only the rate constants from the faster-dissociating phase are used in the main text. The inset shows the complete plot for SRP–RNC_{1A9L} dissociation (Fig. 2 D). The data are representative of >3 experiments. (E) Kinetic simulations of SRP dissociation from Lep50 (i) and nontranslating ribosomes (ii) based on the three-step model and individual rate constants reported by Holtkamp et al. (2012). These simulations show that SRP dissociates from the final, stable RNC–SRP complex at a rate constant (k_{off}) of 0.0058 s^{-1} for RNC bearing a model SRP substrate Lep, and at a k_{off} value of 0.36 s^{-1} from the 70S ribosome. See Materials and methods for details. The data in all the panels are representative of two to three experiments.

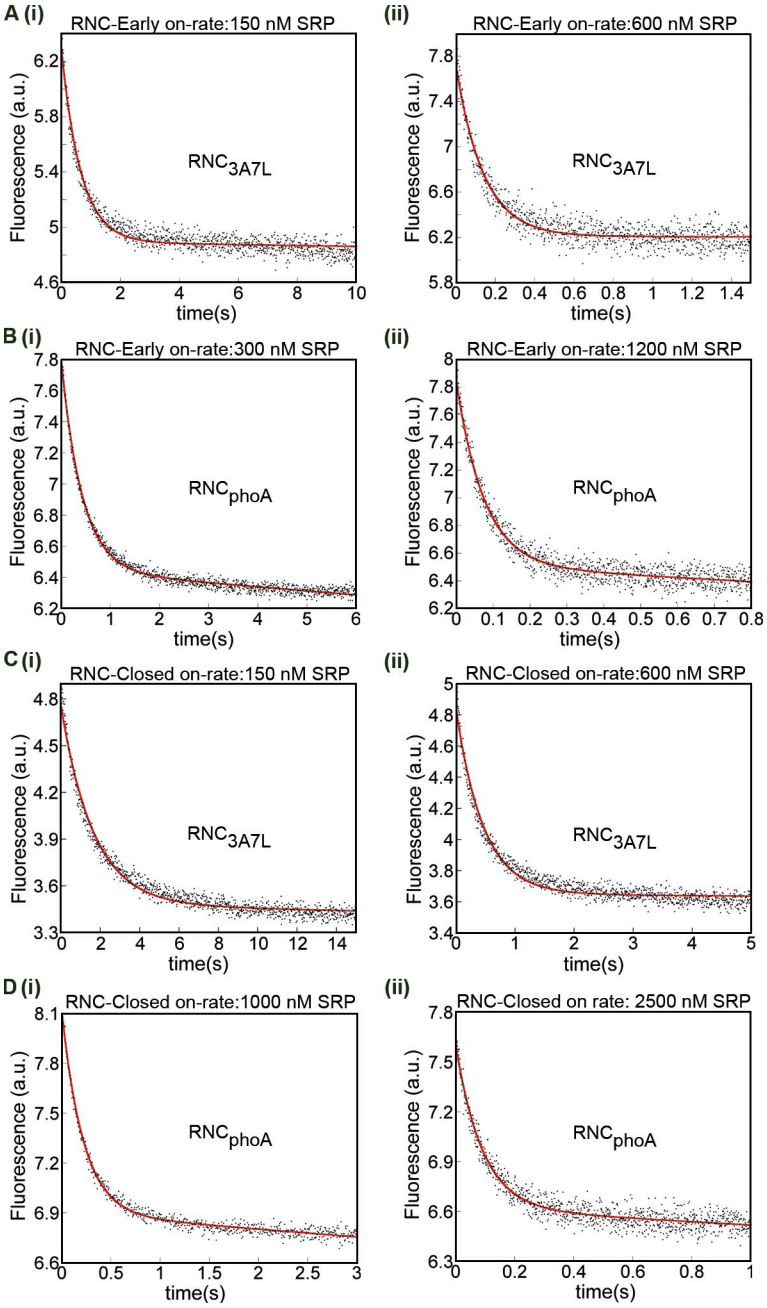

Figure S2. **Representative curves showing the time courses for RNC binding to the SRP–SR early and closed complexes.** The time courses for association of RNCs with the SRP–SR early (A and B) or closed complex (C and D) for RNC_{3A7L} (A and C) and RNC_{phoA} (B and D). The observed rate constants obtained from Eq. 3 were used to generate Fig. 3, B and D. The data in all the panels are representative of two to three experiments.

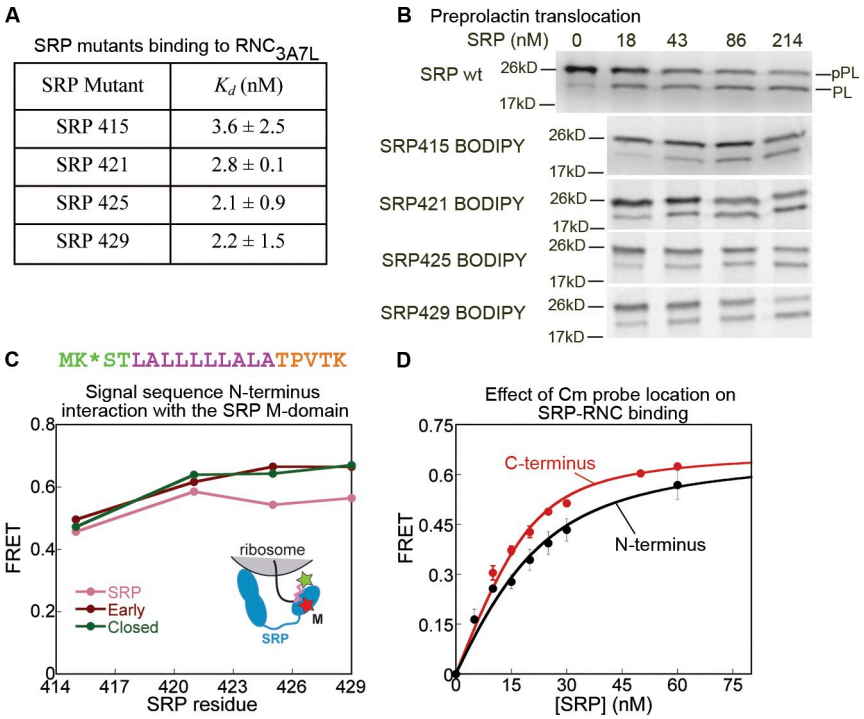

Figure S3. **Signal sequence binding to the SRP M domain.** (A) A summary of the binding dissociation constants obtained for BODIPY-FL–labeled single cysteine mutants of SRP at residues 415, 421, 425, and 429 in the SRP M domain binding to fluorescently labeled RNC_{3A7L}. (B) The activity of BODIPY-FL–labeled single cysteine mutants of SRP was tested in a protein translocation assay (Shan et al., 2007). (C) Maximal FRET efficiency between Cm at the N terminus of signal sequence and BODIPY-FL at the indicated residues in SRP helix M4 upon RNC binding to SRP (pink), and the early (dark red) and closed (green) targeting complexes. The inset shows a diagram of the FRET pair used for this experiment. For clarity, only a part of the ribosome is shown. The location of the donor fluorophore at the N terminus of the signal sequence is shown with an asterisk (top). (D) The binding affinity of SRP, labeled with BODIPY-FL at residue 421, for RNC_{3A7L} labeled with Cm at either the C or N terminus of the signal sequence. The data were fit to Eq. 2 and gave K_d values of 3.7 and 8.4 nM for RNC_{3A7L} labeled at the C and N termini, respectively. Each measurement in C was performed once.

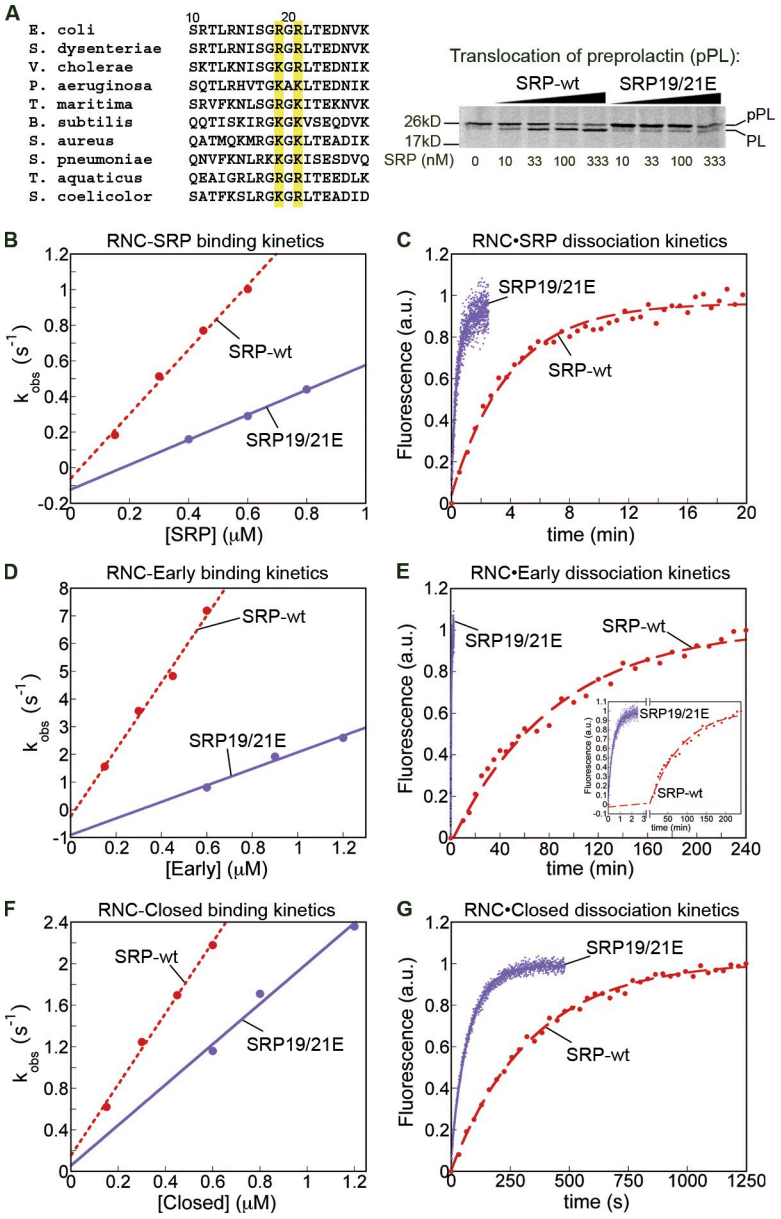

Figure S4. **Sequence information and kinetic data for SRP 19/21E mutant.** (A) Sequence alignment of Ffh homologues with the two conserved basic residues highlighted. Numbering is for *E. coli* Ffh. The right panel shows the activity of the SRP 19/21E mutant in a protein translocation assay (Shan et al., 2007). (B–G) Kinetic measurements for SRP19/21E association with (B, D, and F) and dissociation from RNC_{3A7L} (C, E, and G) at different stages of the targeting pathway. (B and C) SRP only; (D and E) early; (F and G) closed targeting complex. The data for wt SRP (broken lines) are shown for comparison. The rate constants obtained from these data are tabulated in Fig. 4 D. The data in B–G are representative of two to three experiments.

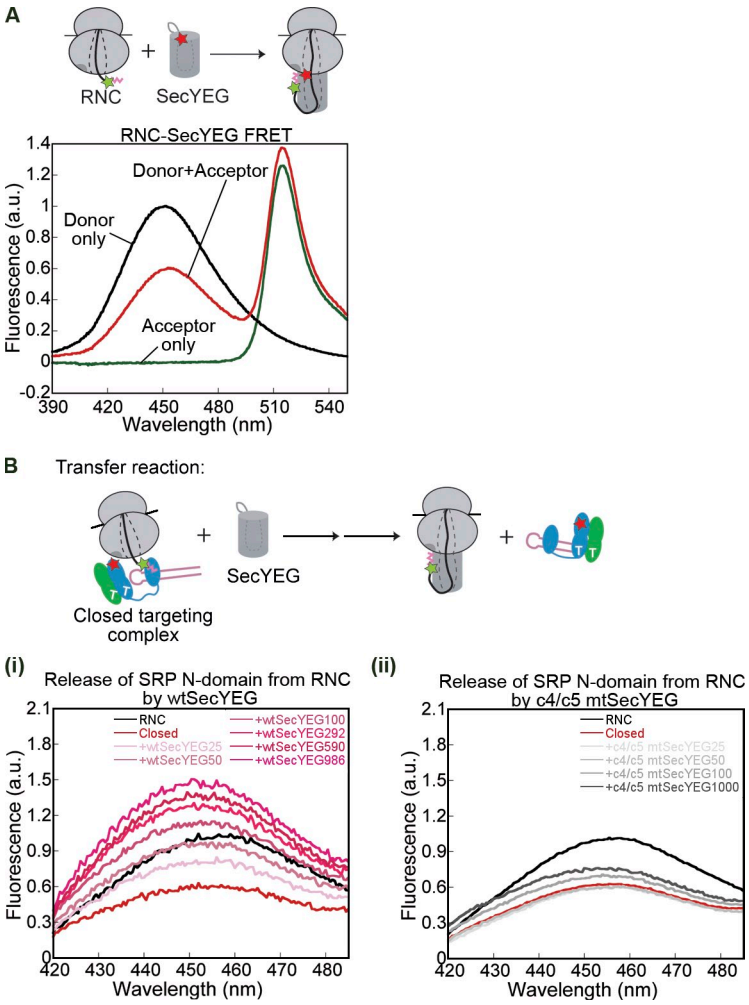

Figure S5. **Cm probe incorporated into the signal sequence reports on RNC–SecYEG binding.** (A) FRET between Cm-labeled RNC and BODIPY-labeled SecYEG. 30 nM SecYEG labeled with BODIPY-FL at residue 180 was added to 40 nM RNC_{3A7L} labeled with Cm at the C terminus. (B) Titration of the closed targeting complex with SecYEG. Wt-SecYEG (i) or c4/c5 mtSecYEG (ii) were titrated into the closed targeting complex containing 20 nM RNC_{3A7L} labeled with Cm at the C terminus, 40 nM SRP labeled with BODIPY-FL at position 11 (N domain), 500 nM FtsY, and 100 µM GppNHp. The fluorescence peak at each concentration was plotted against [SecYEG] to generate Fig. 6 C. In A and B, the schematic shows the binding reaction monitored and the corresponding FRET pair used in the experiment. The data are representative of two to three experiments.

Table S1. **Anisotropy measurements for Cm and BODIPY-FL fluorophores**

Dye	Anisotropy
Cm	0.019
Cm-RNC (C terminus)	0.139
Cm-RNC (N terminus)	0.123
BODIPY-FL	0.011
SRP 415 BODIPY-FL	0.232
SRP 421 BODIPY-FL	0.171
SRP 425 BODIPY-FL	0.205
SRP 429 BODIPY-FL	0.204

References

Holtkamp, W., S. Lee, T. Bornemann, T. Senyushkina, M.V. Rodnina, and W. Wintermeyer. 2012. Dynamic switch of the signal recognition particle from scanning to targeting. *Nat. Struct. Mol. Biol.* 19:1332–1337. http://dx.doi.org/10.1038/nsmb.2421

Shan, S., S. Chandrasekar, and P. Walter. 2007. Conformational changes in the GTPase modules of the signal recognition particle and its receptor drive initiation of protein translocation. *J. Cell Biol.* 178:611–620. http://dx.doi.org/10.1083/jcb.200702018